Tulips University of Tsukuba Repository

Spectrum of slip behaviour in Tohoku fault zone samples at plate tectonic slip rates

著者	Ikari Matt J., Ito Yoshihiro, Ujiie Kohtaro, Kopf Achim J.
journal or publication title	Nature geoscience
volume	8
number	11
page range	870-874
year	2015-11
権利	(C) 2015 Macmillan Publishers Limited.
URL	http://hdl.handle.net/2241/00134950

doi: 10.1038/ngeo2547

Spectrum of slip behavior in Tohoku fault zone samples at plate tectonic slip rates

Matt J. Ikari[1*], Yoshihiro Ito[2], Kohtaro Ujiie[3], Achim J. Kopf[1]

[1]MARUM, Center for Marine Environmental Sciences, University of Bremen, Germany

[2]Disaster Prevention Research Institute, Kyoto University, Japan

[3]Graduate School of Life and Environmental Sciences, University of Tsukuba, Japan

**corresponding author* (mikari@marum.de)

During the 2011 Tohoku-oki earthquake, extremely extensive coseismic slip ruptured shallow parts of the Japan Trench subduction zone and breached the seafloor[6,7]. This part of the subduction zone also hosts slow-slip events[8,9]. The fault thus seems to have a propensity for slip instability or quasi-instability that is unexpected on the shallow portions of important fault zones. Here we use laboratory experiments to slowly shear samples of rock recovered from the Tohoku-oki earthquake fault zone as part of the Japan Trench Fast Drilling project. We find that infrequent perturbations in rock strength appear spontaneously as long-term slow-slip events when the samples are sheared at a constant rate of about 8.5 cm/yr, equivalent to the plate convergence rate. The shear strength of the rock drops by 50 to 120 kPa, which is 3 to 6%, over about 2 to 4 hours. Slip during these events reaches peak velocities of up to 25 cm/yr, similar to slow-slip events observed in several circum-Pacific subduction zones. Furthermore, the sheared samples exhibit the full spectrum of fault-slip behaviors, from fast unstable slip to slow steady creep, which can explain the wide range of slip styles observed in the Japan Trench. We

suggest that the occurrence of slow-slip events at shallow depths may help identify fault segments that are frictionally unstable and susceptible to large coseismic slip propagation.

At the Japan Trench subduction zone, microseismicity observations from ocean bottom seismometers[1], distribution of aftershock hypocentral depths[2,3], and GPS measurements of slip deficit[4] all indicate that the Japan Trench exhibits an "aseismic" zone free of earthquake nucleation at depths shallower than 10 km. This is consistent with the previous conceptual model where the shallowest reaches of subduction megathrusts were considered to be outside the "seismogenic zone" and thus were expected to slip aseismically[5]. However, this view must be revised after the 2011 M_w = 9.0 Tohoku-Oki earthquake at the Japan Trench generated an estimated 50-80 m of coseismic, tsunamigenic slip reaching the seafloor based on geodetic data and repeated bathymetry surveys[6,7]. In addition, the Japan Trench has a long record of slow and tsunamigenic earthquakes at shallow depths in this region[8,9], which is not considered typical of an aseismic, creeping fault zone. Recent evidence thus demonstrates that the near-trench portions of plate-boundary faults can fail in a wide range of slip styles, and an important unresolved question is therefore whether laboratory-measured frictional properties can explain and be used to simulate slip behavior on the shallow Japan Trench megathrust.

Predicting the slip style of faults relies heavily on laboratory friction experiments, which have shown that aseismic slip is favored in materials that strengthen with increased slip velocities (velocity-strengthening friction)[5]. This type of behavior is prevalent in unconsolidated, weak clay-rich sediments[10], which are common in the shallow portions of subduction thrusts[11]. One possible exception is sediment with a high smectite content, which is known to be extremely weak but also exhibits some instances of velocity-weakening friction[12], which is necessary for slip instability. Specifically, velocity weakening in smectite has been observed at low normal stress (< 30 MPa), intermediate sliding velocity (0.2 to 30 μm/s), and room temperature (~20 °C), but under room humidity and not fluid saturated. The origin of velocity weakening in smectite is not well understood.

During Integrated Ocean Drilling Program Expedition 343, the Japan Trench Fast Drilling Project (JFAST), samples of the plate boundary fault zone were recovered ~7 km landward of the Japan Trench axis at 822 meters below seafloor (mbsf), within the region of largest coseismic slip during the 2011 Tohoku earthquake[13] (Figure 1). Mineralogic analyses of the highly deformed, foliated fault zone indicate smectite content of ~80% in the bulk sediment[14]. As expected from previous work on smectite, friction experiments within the range 0.1-30 μm/s indicate that the fault zone is both weak and velocity strengthening but with a few cases of velocity weakening[15], and at coseismic slip velocities of ~1 m/s exhibits very low friction coefficients[16] (μ < 0.2). This seems to indicate potential for slip instability, however pre-earthquake faults are initially moving at plate convergent rates (or slower in cases of full or partial locking), orders of magnitude slower than typical laboratory rates. We investigate here the frictional behavior of the shallow Tohoku megathrust, using slow laboratory experiments conducted at the convergence rate between the Pacific and North American plates of 8.5 cm/yr, or 2.7 nm/s (ref 17) in order to accurately simulate an interseismic megathrust fault zone.

We deform four cylindrical samples (25 mm height, 25 mm diameter): two intact and two powdered core samples from the plate boundary fault zone in a single-direct shear configuration[15] to measure the coefficient of sliding friction $\mu = \tau/\sigma_n'$, where τ is the shear strength and σ_n' is the effective normal stress, and friction velocity dependence $a\text{-}b = \Delta\mu/\Delta\ln v$, where v is the sliding velocity[5]. To approximate in-situ conditions near the trench (assuming hydrostatic pore pressure) samples were sheared at $\sigma_n' = 7$ MPa with 3.5% NaCl brine as pore fluid; samples are allowed fully consolidate prior to shearing so that the pore pressure is assumed negligible. In our tests, we sheared the samples at 10 µm/s for ~5 mm to establish steady-state shear geometry and residual friction level, then subsequently decreased the slip velocity to the plate rate value of 2.7 nm/s, simulating realistically slow initial fault slip rates.

At 10 µm/s we observe a distinct peak in friction of μ = 0.23-0.30 for both powdered and intact samples, that decreases to residual values of ~0.22 for intact and ~0.16 for powdered samples (Figure 2). High-frequency (recurrence ~0.5 s), low-amplitude (10-20 kPa, ~1-2% stress drop) stick-slip behavior is observed upon attainment of residual friction levels. After the decrease in velocity to the plate rate, friction increases to 0.21-0.24 for both intact and powdered samples. Clear stick-slip behavior was initially observed which ceased as friction evolved to a new residual level; stress drops for these events are similar to those at 10 µm/s (~10 kPa, ~ 1%) but have a much longer recurrence (~20 min). The duration of the stick-slip events at both 10 µm/s and 2.7 nm/s is smaller than 0.3 s, our smallest recording interval. Values of *a-b* calculated from the drop from 10 µm/s to 2.7 nm/s range from -0.009 to -0.002; results of 3-fold velocity steps indicate *a-b* = -0.006 to -0.003. This is significantly more velocity weakening than the *a-b* values of -0.001 to 0.003 measured on the same samples at higher rates of 0.1-30 μm/s (ref 15). The observations of velocity-weakening friction and stick-slip behavior clearly demonstrate the propensity for unstable frictional slip, indicating that the shallow megathrust at the Japan Trench is capable of hosting earthquake nucleation in addition to facilitating rupture propagation.

When steady-state strength is re-established following the decrease to the plate rate, shearing proceeds mostly as stable creep. However, larger infrequent strength perturbations spontaneously occur two to three times over several mm (Figure 2), these occur most frequently in tests using intact samples, and were not observed in a control experiment in which powdered Rochester shale was tested as an illite-rich, velocity-strengthening reference material[12]. We observe stress increases before the stress drop so that the friction level before and after the event are similar. Records of shear displacement which have been detrended for the target slip velocity show clear deviations during these events, with a slip deficit occurring during the loading phase and a slip excess occurring during the stress drop. The stress drop for these events ranges from 50-120 kPa, which represents 3-6% of the shear strength. The stress drop occurs over 2-4 hours, with maximum slip rates during these events ranging from 3-8 nm/s (10-25 cm/year).

The larger, irregular events we observe are distinctly different from ordinary stick-slip behavior or slower oscillatory slip[18]. Based on the duration of the stress drop and magnitude of the slip velocity, we interpret these events to be laboratory-generated slow slip events (SSE). These slow events hold several similarities to numerically simulated spontaneous periodic or aperiodic slip transients, including the slip rate, low effective stresses, and conditional stability suggesting that some amount of velocity-weakening friction is necessary[19]. Our observation that stick-slip at the plate rate is only observed during a transient phase of increasing friction following a velocity decrease, and subsequently gives way to a combination of creep and SSE, suggests that the frictional stability of the system evolves toward conditional stability. Considering constant (effective) normal stress, apparatus stiffness, and consistent velocity-weakening we speculate that this evolution may be related to a critical slip distance for dynamic weakening[5]. Because we observe SSE most often in our intact samples, the frictional properties conducive for SSEs may be associated with scaly fabric developed in-situ.

Slow earthquakes and transient slip events observed in natural tectonic settings can vary widely in terms of duration, total slip, and equivalent seismic moment[20]. However, we find that the (maximum) slip velocities we observe, 10-25 cm/yr, are strikingly similar to those of silent earthquakes or SSE observed in several subduction zones[22-30] (Figure 3). Calculated equivalent moment magnitudes of these SSEs range from M_w = 6.6-7.5. A notable feature of most observed natural SSE is that they occur at the lower seismogenic zone boundary or immediately downdip. Our samples were recovered from < 1 km depth at the Japan Trench, consistent with SSEs that occur above or near the shallower updip limit of the seismogenic zone. Shallower SSEs are observed less frequently, but this is likely due to sparser offshore instrumentation and may be more a more common phenomenon. Inversion of GPS data at the northern Costa Rica margin near Nicoya Peninsula reveal two SSEs; one is located at the downdip seismogenic zone boundary at 25-30 km, but another slip patch is observed at ~6 km depth near the updip limit[30]. Ito et al. (2013) observed two SSEs prior to the 2011 Tohoku earthquake; one in

November 2008 (M_w = 6.8) and one in February 2011 (M_w = 7.0) that was likely still ongoing at the time of the earthquake. Slip velocities are estimated to be 360 cm/yr, much faster than the velocities of our laboratory SSE. However, the estimated stress drops of the Tohoku SSE are 50-100 kPa, which match our observed stress drops of 50-120 kPa. Dislocation modeling indicates that these SSE occurred at 10-15 km depth, within the seismogenic zone and co-located with the rupture area of the Tohoku earthquake. We therefore suggest that despite some spatial variations, the entire shallow plate boundary from ~15 km depth to the trench is capable of generating SSEs with an equivalent M_w of ~7.

In addition to producing the SSEs observed prior to the 2011 Tohoku earthquake, the frictional properties of the fault zone likely contributed to large near-trench coseismic slip during the earthquake, either due to active weakening during an SSE[9] or by inherently unstable slip. Most notably this includes evidence of frictional instability (by stick-slip) or capacity for instability (by velocity weakening), but our results also demonstrate that the Tohoku fault zone exhibits the full spectrum of slip behaviors. One important implication is that in the absence of significant seismicity, the occurrence of SSEs on the shallow portions of major faults may be diagnostic of potential slip instability and near-surface coseismic slip in other subduction zones.

Acknowledgements

This research uses samples and/or data provided by the Integrated Ocean Drilling Program (IODP). We are thankful for discussions with the IODP Expedition 343 scientific party, and Heather Savage and an anonymous reviewer for their constructive comments. This work was supported by the Deutsche Forschungsgemeinschaft (DFG) Grant #IK107/1-1 to M.I.

Author contributions

M.I. conducted friction experiments and data analysis. All authors contributed to planning and writing the manuscript.

References

1. Nishizawa, A., Kanazawa, T., Iwasaki, T. & Shimamura, H. Spatial distribution of earthquakes associated with the Pacific plate subduction off northeastern Japan revealed by ocean bottom and land observation. *Phys. Earth Planet. Int.* **75**, 168-175 (1992).
2. Hino, R. et al. Aftershock distribution of the 1994 Sanriku-oki earthquake (M_w 7.7) revealed by ocean bottom seismographic observation. *J. Geophys. Res.* **105**, 21,697-21,710 (2000).
3. Obana, K. et al. Aftershocks near the updip end of the 2011 Tohoku-Oki earthquake. *Earth Planet. Sci. Lett.* **382**, 111-116 (2013).
4. Hashimoto, C., Noda, A., Sagiya, T. & Matsu'ura, M. Interplate seismogenic zones along the Kuril-Japan trench inferred from GPS data inversion. *Nat. Geosci.* **2**, 141-144 (2009).
5. Scholz, C.H. Earthquakes and friction laws. *Nature* **391**, 37-42 (1998).
6. Fujiwara, T. et al. The 2011 Tohoku-Oki earthquake: Displacement reaching the trench axis. *Science* **334**, 1240 (2011).

7. Ito, Y. et al. Frontal wedge deformation near the source region of the 2011 Tohoku-Oki earthquake. *Geophys. Res. Lett.* **38**, L00G05 (2011).

8. Fukao, Y. & Kanjo, K. A zone of low-frequency earthquakes beneath the inner wall of the Japan Trench. *Tectonophys*. **67**, 153-162 (1980).

9. Ito, Y. et al. Episodic slow slip events in the Japan subduction zone before the 2011 Tohoku-Oki earthquake. *Tectonophys*. **600**, 14-26 (2013).

10. Ikari, M.J., Saffer, D.M. & Marone, C. Frictional and hydrologic properties of clay-rich fault gouge. *J. Geophys. Res.* **114**, B05409 (2009).

11. Underwood, M.B. in *The Seismogenic Zone of Subduction Thrust Faults* (eds. Dixon, T.H. & Moore, J.C.) 42-84 (2007)

12. Saffer, D.M., & Marone, C. Comparison of smectite- and illite-rich gouge frictional properties: application to the updip limit of the seismogenic zone along subduction megathrusts. *Earth Planet. Sci. Lett.* **215**, 219-235 (2003).

13. Chester, F.M., Mori, J.J., Eguchi, N., Toczko, S. & Expedition 343/343T Scientists. *Proc. IODP*, **343/343T**: Integrated Ocean Drilling Program Management International, Inc., Tokyo (2013).

14. Kameda, J. et al. Pelagic smectite as an important factor in tsunamigenic slip along the Japan Trench. *Geology* (2015).

15. Ikari, M.J., Kameda, J., Saffer, D.M. & Kopf, A.J. Strength characteristics of Japan Trench borehole samples in the high-slip region of the 2011 Tohoku-Oki earthquake. *Earth Planet. Sci. Lett.* **412**, 35-41 (2015).

16. Ujiie, K. et al. Low coseismic shear stress on the Tohoku-Oki megathrust determined from laboratory experiments. *Science* **342**, 1211-1214 (2013).

17. DeMets, C., Gordon, R.G., Argus, D.F. & Stein, S. Effect of recent revisions to the geomagnetic reversal time scale on estimates of current plate motions. *Geophys. Res. Lett.* **21**, 2191-2194 (1994).

18. Baumberger, T., Berthoud, P. & Caroli, C. Physical analysis of state- and rate-dependent friction law II: Dynamic friction. *Phys. Rev. B* **60**, 3928-3939 (1999).

19. Liu, Y. & Rice, J.R. Spontaneous and triggered aseismic deformation transients in a subduction fault model. *J. Geophys. Res.* **112**, B09404 (2007).

20. Ide, S., Beroza, G.C., Shelly, D.R. & Uchide, T. A scaling law for slow earthquakes. *Nature* **447**, 76-79 (2007).

21. Kostoglodov, V. et al. A large silent earthquake in the Guerrero seismic gap, Mexico. *Geophys. Res. Lett.* **30**, 1807 (2003).

22. Hirose, H., Hirahara, K., Kimata, F., Fujii, N. & Miyazaki, S. A slow thrust slip event following the two 1996 Hyuganada earthquakes beneath the Bungo Channel, southwest Japan. *Geophys. Res. Lett.* **21**, 3237-3240 (1999).

23. Hirose, H. & Obara, K. Repeating short- and long-term slow slip events with deep tremor activity around the Bungo channel region, southwest Japan. *Earth Plan. Space* **57**, 961-972 (2005).

24. Miyazaki, S., Segall, P., McGuire, J.J., Kato, T. & Hatanaka, Y. Spatial and temporal evolution of stress and slip rate during the 2000 Tokai slow earthquake. *J. Geophys. Res.* **111**, B03409 (2006).

25. Wallace, L.M. & Beavan, J. A large slow slip event on the central Hikurangi subduction interface beneath the Manawatu region, North Island, New Zealand. *Geophys. Res. Lett.* **33**, L11301 (2006).

26. Douglas, A., Beavan, J., Wallace, L. & Townend, J. Slow slip on the northern Hikurangi subduction interface, New Zealand. *Geophys. Res. Lett.* **32**, L16305 (2005).

27. Ohta, Y., Freymuller, J.T., Hreinsdóttir, S. & Suito, H. A large slow slip event and the depth of the seismogenic zone in the south central Alaska subduction zone. *Earth Planet. Sci. Lett.* **247**, 108-116 (2006).

28. Rogers, G. & Dragert, H. Episodic tremor and slip on the Cascadia subduction zone: The chatter of silent slip. *Science* **300**, 1942-1943 (2003).

29. Szeliga, W., Melbourne, T., Santillan, M. & Miller, M. GPS constraints on 34 slow slip events within the Cascadia subduction zone. *J. Geophys. Res.* **113**, B04404 (2008).

30. Outerbridge, K.C. et al. A tremor and slip event on the Cocos-Caribbean subduction zone as measured by a global positioning system (GPS) and seismic network on the Nicoya Peninsula, Costa Rica. *J. Geophys. Res.* **115**, B10408 (2010).

Figure Captions

Figure 1: Overview of the Tohoku Region of the Japan Trench. (Top Left) Map of the Japan Trench area showing the locations of the JFAST drilling site C0019 (circle) and seismic line HD33B (line within circle)[13]. Star indicates location of the M_w = 9.0 Tohoku earthquake. White bar indicates region of ~50 m coseismic slip from bathymetry data[6]. Dashed box indicates area of the M_w = 7.0 2011 SSE preceding the Tohoku earthquake[9].

(Bottom) Seismic reflection profile for line HD33B[13]. (Top Right) Photo of a section from Core 17R-1, the plate boundary fault zone. Scale at left in cm.

Figure 2: Summary of Experimental Results. (a) Example of shear stress and friction data for an intact sample of the JFAST plate boundary fault zone (Core 17R-1). Boxes and arrows indicate close-up views in following panels (b) Close-up view of friction data showing the decrease from 10 μm/s to 2.7 nm/s. $\Delta\mu_{ss}$ indicates the change in steady-state friction used to calculate *a-b*. Box indicates the close-up view shown in panel c. (c) Close-up view of stick-slip behavior, showing shear stress and displacement as a function of time. Advances in displacement correlate with stress drops. (d) Close-up of 3-fold increases in velocity. Inset shows a closeup view the 8.1 to 27 nm/s velocity step data, overlain by an inverse model from which the value *a-b* = 0.0034 is obtained. (e) The first slow instability in panel a, showing the shear stress (top), displacement of the sample detrended for the remotely imposed slip velocity of 2.7 nm/s (middle), and the time-averaged instantaneous real slip velocity of the sample (bottom) as a function of time. $\Delta\tau$ = stress drop. Detrended displacement set to 0 at the beginning of the event loadup phase, decreasing values indicate slip deficit and positive values indicates slip accumulation. Solid line on the velocity plot indicates prescribed driving velocity of 2.7 nm/s for comparison. (f) Same as panel e, for the second slow instability in panel a.

Figure 3: Comparison of laboratory and natural SSE. Slip velocity and duration of laboratory SSE observed in JFAST samples compared with a selection of natural subduction zone SSE[2] in Guerrero, Mexico[21], the Bungo Channel (both short and long-term SSE)[22,23] and eastern Nankai Trough (Tokai region) offshore Japan[24], the Hikurangi subduction zone offshore New Zealand near Manuwatu[25] and Gisborne[26], southern

Alaska[27], Cascadia[28,29], and the Nicoya Peninsula, Costa Rica[30]. *The total slip during our laboratory SSEs is probably limited by sample size, but using our laboratory-observed SSE slip velocities and assuming typically observed slip magnitudes of 2-20 cm results in event durations that match natural SSE.

Methods

We tested four samples in this study: two intact samples, and two powdered gouges. The intact samples were trimmed from whole-round cores parallel to the core axis, so that the fabric is aligned with the plane of shear. The powdered gouges were prepared by air drying fragments of the whole-round core, which were then crushed with a mortar and pestle to a grain size < 125 μm. The powders were then mixed with simulated seawater (3.5% NaCl brine) into a stiff paste and cold-pressed into the sample cell, which houses a cylindrical volume (25 mm diameter, 30 mm height). Both powdered and intact samples were tested with the sample cell flooded with seawater and thus tested in a fluid-saturated condition. The samples are confined by the sample cell and are not jacketed. All tests were performed at a constant temperature (~20 °C) in a climate-controlled room.

We conducted our experiments using a Giesa RS5 direct shear apparatus[31] (Supp. Figure 1). The sample cell is a stack of two steel plates which houses the cylindrical sample. Normal load is applied to the top face of the sample with a vertical ram, and held constant in servo-control via a proportional-integrative-derivative controller. We applied a normal stress of 7 MPa, comparable to in-situ effective stresses at the depth of sample recovery estimated from shipboard moisture and density measurements[13]. The sample was then allowed to consolidate overnight (~18 hours) and is allowed to drain at the top and bottom faces via porous metal frits; the top is open to the atmosphere and the bottom to an open pore fluid reservoir within which the sample cell sits to prevent desiccation. Although we do not directly control the pore pressure, shearing was initiated after the compaction rate, measured as change in sample height over time, became negligible. We therefore assume that any excess pore pressure that may have developed during loading dissipates during the consolidation process and the applied stress equals the effective normal stress acting on the sample (pore pressure = 0). We further assume that because the sample maintains zero pore pressure during the experiment, the frictional behavior we observe is not attributable to fluctuations in said pressure.

The lower plate is displaced horizontally relative to the top plate by an electric motor, inducing planar (i.e. localized) shear deformation in the sample. The shear resisting force of the interface between the two plates is ~9 N, which we correct for in our measurements. For our samples, which have an area of 5.07×10^{-4} m^2, the resolution of the load cells is 0.30 kPa in normal stress and 0.15 kPa in shear stress. Fluctuations due to electrical noise are estimated to be +/- ~0.4 µm and +/- ~2 kPa. Displacement is measured directly at the sample cell by a potentiometric sensor with a resolution of 0.8 µm. Because the horizontal displacement sensor is located directly at the sample cell (rather than at the load cell) the recorded shear displacement represents the displacement of the sample without effects of apparatus stiffness. However, we also measure the apparatus stiffness by placing a separate displacement sensor at the horizontal load cell. Under a normal stress of 7 MPa, the horizontal stiffness is 3.8 kN/mm. The stiffness of the apparatus was not modified for these experiments. The displacement record at the sample cell is a measured value, which is distinct from the driving velocity enforced by the motor near the load cell. We utilize a stepper motor with an update rate of 0.19 Hz and a step width of 0.015 µm, and recorded our data at 0.033 Hz (or 10 measurements every 0.81 µm defined by the displacement sensor resolution) for a time-averaged displacement rate of 2.7 nm/s.

We measure the shear strength τ throughout the experiment, which we use to calculate an apparent friction coefficient μ:

$$\mu = \frac{\tau}{\sigma_n}, \quad (1)$$

Assuming (1) that the cohesion is negligible, and (2) that any pore pressure fluctuations are small so that the applied normal stress equals the effective normal stress throughout the experiment.

We measure the velocity-dependence of friction as:

$$a - b = \frac{\Delta\mu_{ss}}{\Delta \ln V} \quad (2)$$

where $\Delta\mu_{ss}$ is the difference in steady-state friction before and after a change in slip velocity V. Determination of steady-state is an approximation by which no obvious slip-hardening or weakening trends are present where the measurement is made. For the decrease in slip velocity from the background rate of 10 µm/s to the plate-rate of 2.7 nm/s, we calculate a-b by directly measuring $\Delta\mu_{ss}$. We also conducted velocity-stepping tests using three-fold (half-order of magnitude) increases in slip velocity at 2.7, 8.1, 27, and 81 nm/s. The frictional response to a velocity step is described by the RSF relations:

$$\mu = \mu_o + a\ln\left(\frac{V}{V_o}\right) + b_1 \ln\left(\frac{V_o\theta_1}{D_{c1}}\right) + b_2 \ln\left(\frac{V_o\theta_2}{D_{c2}}\right) \quad (2)$$

$$\frac{d\theta_i}{dt} = 1 - \frac{V\theta_i}{D_{c\,i}}, i = 1,2 \qquad (3)$$

Where a, b_1 and b_2 are dimensionless constants, θ_1 and θ_2 are state variables (units of time), and D_{c1} and D_{c2} are critical slip distances over which friction evolves to a new steady state value[32]. If the data are well described by a single state variable then D_{c1} = D_{c2} and we take $b_2 = 0$; to account for the possibility of one or two state variables we define $b = b_1 + b_2$. Equation 3 describes the evolution of the state variable θ and is known as the "Dieterich" or "slowness" law, which has the property that friction can change as a function of time even in the limiting case of zero slip velocity[32]. The individual RSF parameters a, b_1, b_2, D_{c1} and D_{c2} must be determined by inverse modeling using an iterative least-squares method that also accounts for elastic interaction with the testing machine[33,34]. This requires an expression for the system stiffness k (friction/displacement):

$$\frac{d\mu}{dt} = k(V_{lp} - V)\,. \qquad (5)$$

Conventionally, (V_{lp}-V) is defined as the difference between true fault slip velocity V and the remotely recorded load point velocity V_{lp}, and k is the stiffness of the testing machine, which includes the forcing blocks and support structure, and the fault zone of finite width. For our apparatus stiffness (3.8 kN/mm) and sample dimensions ($5\text{x}10^{-4}$ m^2) this results in k = ~1 mm^{-1}. Our modeling procedure also allows the removal of long-term slip-dependent friction trends, in order to avoid biasing and more accurately determine the friction velocity dependence[34]. Although the modeling technique is a more robust method of determining a-b, it is difficult to apply to large, negative velocity differences and therefore was not used for the decrease from the background velocity to plate convergence velocity.

Methods References:

31. Ikari, M.J., Hüpers, A., & Kopf, A.J. Shear strength of sediments approaching subduction in the Nankai Trough, Japan as constraints on forearc mechanics. *Geochem. Geophys. Geosyst.* **14**, 2716-2730 (2013).

32. Dieterich, J.H. in *Mechanical Behavior of Crustal Rocks* Vol. 24 (eds. Carter, N.L. et al.) 102-120 (Geophys. Monogr, Ser., 1981).

33. Reinen, L.A. & Weeks, J.D. Determination of rock friction constitutive parameters using an iterative least squares inversion method. *J. Geophys. Res.* **98**, 15,937-15,950 (1993).

34. Blanpied, M.L., Marone, C.J., Lockner, D.A., Byerlee, J.D. & King, D.P. Quantitative measure of the variation in fault rheology due to fluid-rock interactions. *J. Geophys. Res.* **103**, 9691-9712 (1998).

Supplementary Figure 1: Schematic diagram of the single-direct shear apparatus. Not to scale.

Supplementary Figure 2: Coefficient of friction as a function of shear displacement for tests on intact JFAST fault zone samples in this study. Velocity steps were performed in experiment B384, which is also shown in main text Figure 2.

Supplementary Figure 3: Coefficient of friction as a function of shear displacement for tests on powdered JFAST fault zone samples in this study. Velocity steps were performed in experiment B525. Significant slip weakening at the end of the tests with powdered samples is attributed to sample extrusion from the testing cell. Note that SSE occur far less frequently in powdered samples.

Supplementary Figure 4: Coefficient of friction as a function of shear displacement for samples of Rochester shale as a control experiment for comparison (B524), prepared in an identical manner to the JFAST samples. Of note: (1) no SSE-type shear stress excursions occur at 2.7 nm/s for this material, (2) no stick-slip occurs in this material, (3) friction decreases following the decrease in slip velocity, signifying velocity-strengthening friction, and (4) velocity-steps (positive increases in velocity) also indicate velocity-strengthening friction.

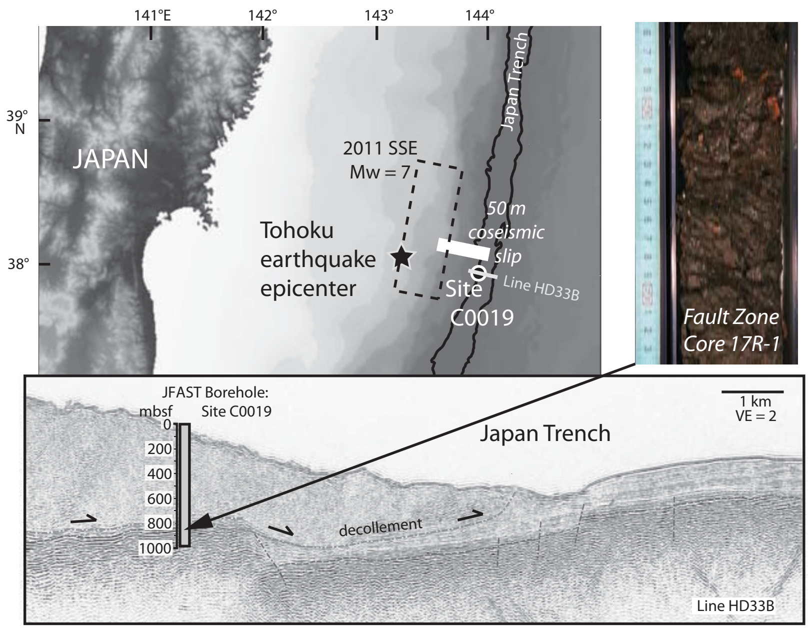

Figure 1: Ikari et al., Japan Trench Instability

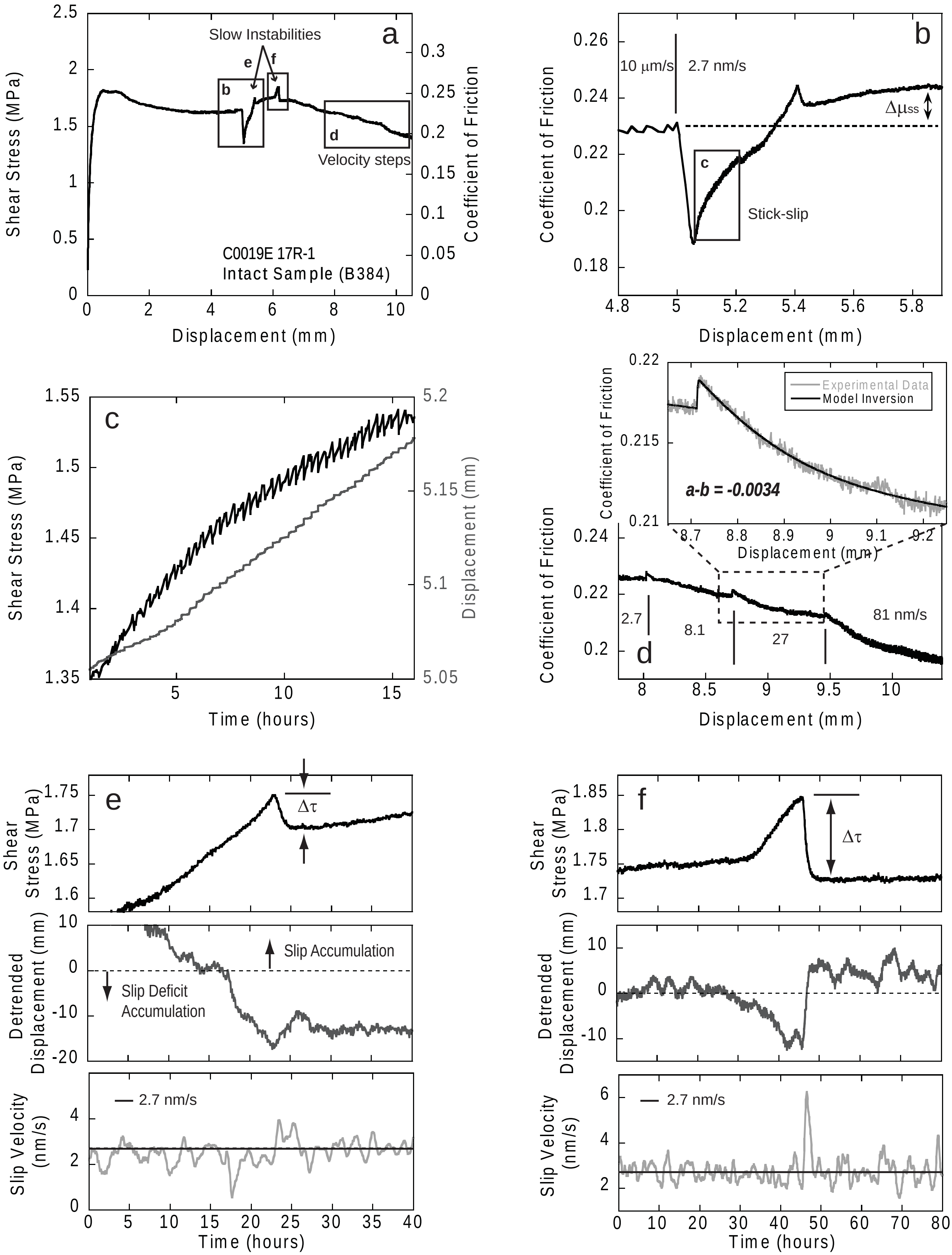

Figure 2: Ikari et al., Japan Trench Instability

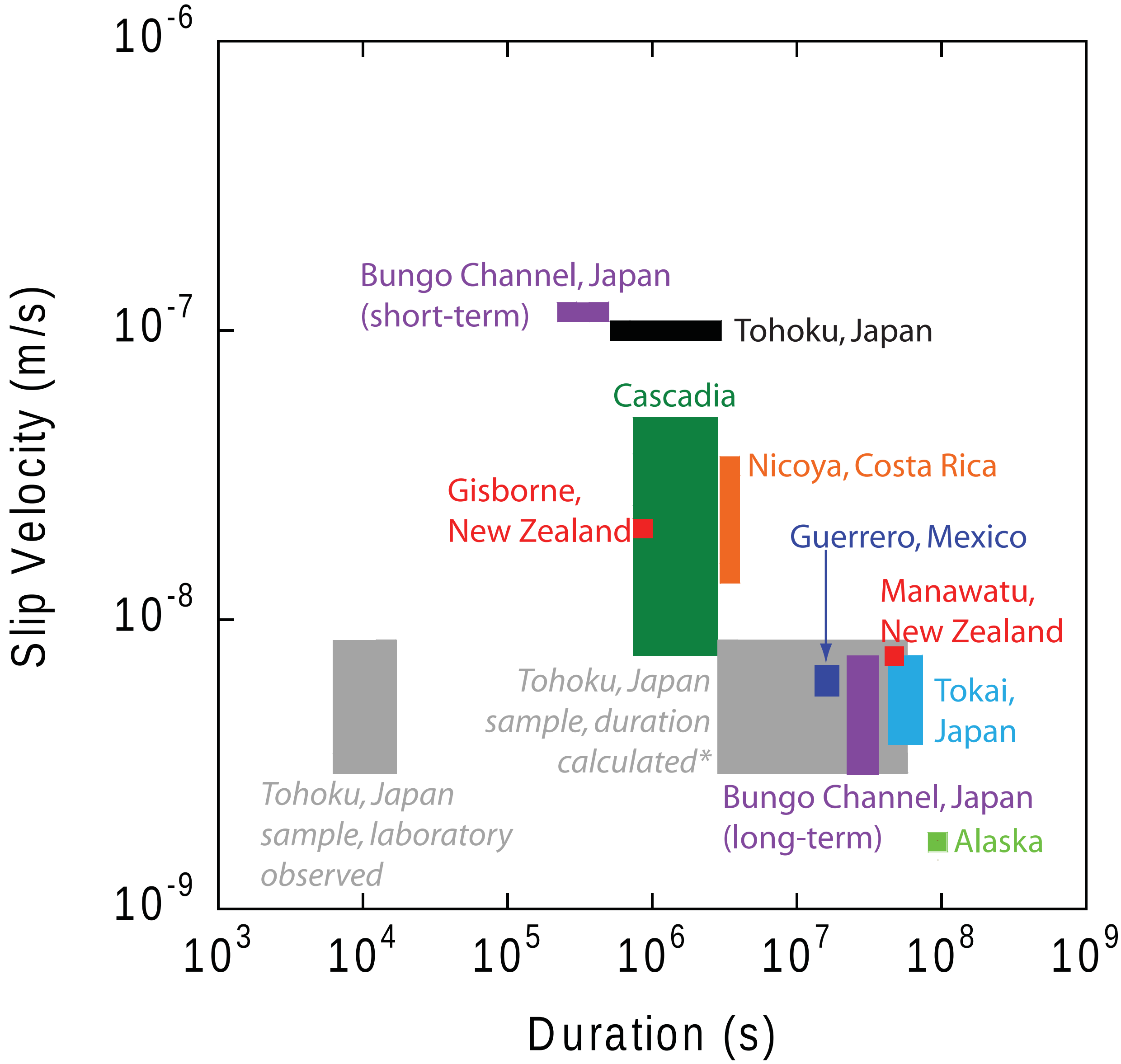

Figure 3: Ikari et al., Japan Trench Instability